Heptacoordination: Pentagonal Bipyramidal XeF_7^+ and TeF_7^- Ions

Karl O. Christe,*,† David A. Dixon,‡ Jeremy C. P. Sanders,§ Gary J. Schrobilgen,*,§ and William W. Wilson†

Contribution from the Rocketdyne Division of Rockwell International Corporation, Canoga Park, California 91309, Central Research and Development Department, E. I. du Pont de Nemours and Company, Inc., Experimental Station, Wilmington, Delaware 19880-0328, and Department of Chemistry, McMaster University, Hamilton, Ontario L8S 4M1, Canada

Received February 18, 1993⊛

Abstract: The TeF_7^- anion was studied experimentally by vibrational and ^{19}F and ^{125}Te NMR spectroscopy. Ab initio calculations employing effective core potentials and density functional theory calculations at the self-consistent nonlocal level with the nonlocal exchange potential of Becke and the nonlocal correlation functional of Perdew were used for the analysis of the isoelectronic series TeF_7^-, IF_7, XeF_7^+. It is shown that XeF_7^+ is a stable structure, that all three members of this series possess a pentagonal bipyramidal equilibrium geometry, and that from the two closest lying saddle point geometries only the monocapped trigonal prism, but not the monocapped octahedron, is a transition state for the intramolecular axial–equatorial ligand exchange. The results from a normal coordinate analysis reveal the existence of an unusual new effect which counteracts the ligand–ligand repulsion effect and is characterized by axial bond stretching encouraging equatorial bond stretching. While in TeF_7^- the ligand–ligand repulsion effect dominates, in XeF_7^+ the new effect becomes preponderant.

Introduction

The problems associated with heptacoordination are manifold and fascinating[1-5] and have recently received significant renewed interest.[3-11] On the basis of the hard sphere model of the valence shell electron pair repulsion (VSEPR) rules of repelling points on a sphere, the energetically preferred structure for a heptacoordinated species is a monocapped octahedron.[1,2] Two other structures that are only slightly higher in energy are those of a monocapped trigonal prism and a pentagonal bipyramid.[12-15] A study of the relative total repulsive force between seven repelling points of a sphere in terms of the energy law

$$E = \sum_{i \neq j} \frac{1}{r_{ij}^{\,n}} \qquad (1)$$

where r_{ij} is the distance between two of the points and n is an unknown constant, has indicated[13-15] that the minimum energy structure of these heptacoordinated species is a function of n. For $0 < n < 3$, i.e., soft repulsion, the pentagonal bipyramid is the minimum energy structure, while for $3 < n < 6$, the monocapped trigonal prism, and for $n > 6$, i.e., hard repulsion, the monocapped octahedron are the energetically favored structures. Whereas these predictions seem to hold well for heptacoordinated transition-metal compounds,[10] the presently known heptacoordinated main-group compounds, in spite of their expected pronounced hardness, show a strong preference for pentagonal bipyramidal structures.[3,4,6-10] In view of these findings it was of interest to study the isoelectronic series of main-group species XeF_7^+, IF_7, TeF_7^-, in which the hardness should increase from TeF_7^- to XeF_7^+.

For the XeF_7^+, IF_7, TeF_7^- series, the following information was previously available. For XeF_7^+, no previous reports could be found in the literature. The IF_7 molecule has been known and studied since 1931,[16] but a better understanding of its characteristic behavior was achieved only very recently.[3] The TeF_7^- anion has been known since 1957,[17,18] but again this anion was not well characterized. Whereas some preliminary results on TeF_7^- were recently published in three short notes,[7-9] a full account and analysis of the data have not been presented before and the vibrational assignments needed revision.

In this paper, we present data on the novel XeF_7^+ cation and a complete analysis of the TeF_7^- anion that firmly establishes the vibrational assignments for the isoelectronic XeF_7^+, IF_7, TeF_7^- series. This analysis resulted in the discovery of a highly unusual reversal of Raman intensities in the A_1' symmetry block which contains only two orthogonal and, hence, normally very weakly coupled stretching modes. By means of a normal coordinate analysis, the cause of this intensity reversal was identified and is attributed to a novel effect which counteracts the ligand–ligand repulsion effect. Furthermore, ab initio and density functional

† Rocketdyne.
‡ Du Pont.
§ McMaster University.
⊛ Abstract published in *Advance ACS Abstracts*, September 1, 1993.

(1) Gillespie, R. J. *Molecular Geometry*; Van Nostrand Reinhold Company: London, 1972.
(2) Gillespie, R. J.; Hargittai, I. *The VSEPR Model of Molecular Geometry*; Allyn and Bacon, A Division of Simon & Schuster, Inc.: Needham Heights, MA, 1991.
(3) Christe, K. O.; Curtis, E. C.; Dixon, D. A. *J. Am. Chem. Soc.* **1993**, *115*, 1520.
(4) Christe, K. O.; Dixon, D. A.; Mahjoub, A. R.; Mercier, H. P. A.; Sanders, J. C. P.; Seppelt, K.; Schrobilgen, G. J.; Wilson, W. W. *J. Am. Chem. Soc.* **1993**, *115*, 2696.
(5) Gillespie, R. J. *Chem. Soc. Rev.* **1992**, 59.
(6) Christe, K. O.; Christe, E. C.; Dixon, D. A.; Mercier, H. C. P.; Sanders, J. C. P.; Schrobilgen, G. J. *J. Am. Chem. Soc.* **1991**, *113*, 3351.
(7) Christe, K. O.; Sanders, J. C. P.; Schrobilgen, G. J.; Wilson, W. W. *J. Chem. Soc., Chem. Commun.* **1991**, 837.
(8) Mahjoub, A. R.; Seppelt, K. *J. Chem. Soc., Chem. Commun.* **1991**, 840.
(9) Mahjoub, A. R.; Drews, T.; Seppelt, K. *Angew. Chem., Int. Ed. Engl.* **1992**, *31*, 1036.
(10) Christe, K. O.; Dixon, D. A.; Sanders, J. C. P.; Schrobilgen, G. J.; Wilson, W. W. *Inorg. Chem.*, in press.
(11) Mahjoub, A. R.; Seppelt, K. *Angew. Chem., Int. Ed. Engl.* **1991**, *30*, 323.
(12) (a) Hoffmann, R.; Beier, B. F.; Muetterties, E. L.; Rossi, A. R. *Inorg. Chem.* **1977**, *16*, 511. (b) Kepert, D. *Inorganic Stereochemistry*; Springer: Berlin, 1982.
(13) Claxton, T. A.; Benson, G. C. *Can. J. Chem.* **1966**, *44*, 157.
(14) Bradford Thompson, H.; Bartell, L. S. *Inorg. Chem.* **1968**, 7, 488.
(15) McDowell, H. K.; Chiu, H.-L.; Geldard, J. F. *Inorg. Chem.* **1988**, *27*, 1674.
(16) Ruff, O.; Keim, R. Z. *Anorg. Chem.* **1931**, 201, 245.
(17) Muetterties, E. L. *J. Am. Chem. Soc.* –1957, *79*, 1004.
(18) Selig, H.; Sarig, S.; Abramowitz, S. *Inorg. Chem.* **1974**, *13*, 1508.

0002-7863/93/1515-9461$04.00/0

theory calculations were used to determine the relative energies, minimum energy structures, saddle points, and transition states of the XeF_7^+, IF_7, TeF_7^- series. This work completes our systematic study of these and similar heptacoordinated main-group element compounds.[3,4,6,7,10]

Experimental Section

Apparatus and Materials. Volatile materials were handled in stainless steel–Teflon and Pyrex glass vacuum lines, as described previously.[6] Nonvolatile materials were handled in the dry nitrogen atmosphere of a glovebox (Vacuum Atmospheres Model DLX).

Literature methods were used for the syntheses of $N(CH_3)_4F$[19] and TeF_4[20] and the drying of CH_3CN (Caledon).[21] Tellurium hexafluoride was prepared by fluorination of crude TeF_4 in a Monel reactor using a 50 mol % excess of elemental fluorine under autogeneous pressure at 250 °C for 4 h. Crude TeF_6 was purified by condensation onto a dry sample of NaF in a stainless steel Whitey cylinder at −196 °C and stored at room temperature for several days prior to use.

Synthesis of $N(CH_3)_4TeF_7$. Anhydrous tetramethylammonium fluoride (0.5125 g, 5.5022 mmol) was loaded into a $^1/_2$-in. o.d. Teflon–FEP tube in the drybox. The tube was equipped with a Kel-F valve and attached to a glass vacuum line. Anhydrous CH_3CN (ca. 3 mL) was distilled onto the $N(CH_3)_4F$ at −196 °C. The mixture was warmed briefly to 25 °C in order to dissolve the $N(CH_3)_4F$, frozen to −78 °C, and pressurized with dry N_2 (1.5 atm). The tube was attached to the metal vacuum line and evacuated at −196 °C. Tellurium hexafluoride (5.75 mmol, 4.5 mol % excess) was metered out into the calibrated vacuum line and condensed into the FEP tube at −196 °C. The reaction mixture was warmed to −40 °C and agitated as the CH_3CN and TeF_6 melted. The reaction took place with formation of a white precipitate. In order to ensure that the reaction was complete, the mixture was warmed to 25 °C and allowed to stand at this temperature for 10 min. The excess TeF_6 and CH_3CN solvent were pumped off in a dynamic vacuum, leaving the $N(CH_3)_4TeF_7$ as a dense white powder (1.7208 g, 93%).

Nuclear Magnetic Resonance Spectroscopy. The ^{19}F and ^{125}Te NMR spectra were recorded unlocked (field drift <0.1 Hz h^{-1}) on a Bruker AM-500 spectrometer equipped with an 11.744-T cryomagnet. The ^{19}F spectra were obtained using a 5-mm combination $^1H/^{19}F$ probe operating at 470.599 MHz. The spectra were recorded in a 32K memory. A spectral width setting of 5000 Hz was employed, yielding a data point resolution of 0.305 Hz/data point and an acquisition time of 3.28 s. No relaxation delays were applied. Prior to Fourier transformation, the free induction decay was zero-filled to 128K of memory, giving a data point resolution of 0.076 Hz/data point. Typically, 16 transients were accumulated. The pulse width corresponding to a bulk magnetization tip angle, θ, of approximately 90° was equal to 1 μs. No line broadening parameters were used in the experimental multiplication of the free induction decays prior to Fourier transformation.

The ^{125}Te NMR spectra were obtained at 157.794 MHz by using a broad-band VSP probe tunable over the range 23-202 MHz. The spectra were recorded in a 32K memory. The spectral width setting was 25 kHz, which yielded a data point resolution of 1.526 Hz/data point and an acquisition time of 0.655 s. Prior to Fourier transformation, the free induction decay was zero-filled to 64K of memory, giving a data point resolution of 0.763 Hz/data point. No relaxation delays were applied. Typically 5000 transients were accumulated. The pulse width corresponding to a bulk magnetization tip angle, θ, of approximately 90° was equal to 10 μs. A line broadening parameter of 1.5 Hz was applied to the exponential multiplication of the free induction decay prior to Fourier transformation.

The spectra were referenced to neat external samples of $CFCl_3$(^{19}F) and $(CH_3)_2Te$(^{125}Te) at ambient temperature. The chemical shift convention used is that a positive sign signifies a chemical shift to high frequency of the reference compound.

NMR samples were prepared in 10- or 5-mm precision glass tubes (Wilmad). Solids were weighed into the tubes in the drybox, and CH_3CN solvent was distilled in vacuo onto the solid at −78 °C. The tubes were flame-sealed in a dynamic vacuum while keeping the contents frozen at −78 °C.

Vibrational Spectra. Infrared spectra of solid $N(CH_3)_4TeF_7$ were recorded on a Perkin-Elmer Model 283 spectrometer. The finely powdered sample was pressed between two AgBr disks in a Wilks minipress inside the drybox. Raman spectra were recorded on a Spex Model 1403 spectrophotometer using the 647.1-nm exciting line of a Kr ion laser and baked-out Pyrex melting point capillaries as sample containers.

Computational Methods. The electronic structure calculations were done by both ab initio molecular orbital and density functional theories. At the ab initio molecular orbital level effective core potentials (ECP) were used for the core electrons on the central atoms. The valence basis sets are of polarized double-ϑ quality. The fluorine basis set is from Dunning and Hay,[22] and the ECP, from Wadt and Hay,[23] including relativistic corrections and augmented by a d function on the central atom.[24] The geometries were optimized by using analytic gradient techniques[25] at the SCF level.[26] Final energies were calculated for the SCF geometries at the MP-2 level. The force fields were calculated analytically.[27,28] The ab initio MO calculations were done with the program GRADSCF,[29] as implemented on a Cray YMP computer system. This computational method generally underestimates these central atom–fluorine bond distances by about 0.01–0.02 Å and, hence, results in vibrational frequency and force constant values which are somewhat too high. Therefore, the calculated values were scaled using empirical factors to give the best fit between calculated and observed frequencies. If the deformation frequencies showed significantly larger deviations than the stretching frequencies, separate scaling factors were used for the two groups.[30] Since the force constants are proportional to the square of the frequencies, the calculated force constants were scaled by the square of the factors used for scaling the corresponding frequencies.

The density functional theory (DFT)[31] calculations were done with the program DGauss,[32] which employs Gaussian orbitals on a Cray YMP computer. Norm-conserving pseudopotentials[33] were generated for I, the Te set for I, Te, and Xe by following the work of Troullier and Martins.[34] The valence basis set for I is [421/31/1] with a fitting basis set of [7/6/1], and the corresponding basis sets for Te and Xe have the form (42/43/1) with a [7/5] fitting basis. The basis set for F is of polarized triple-ζ valence quality and has the form (7111/411/1) with a [7/3/3] fitting basis.[35] The calculations were done with the local

(19) Christe, K. O.; Wilson, W. W.; Wilson, R. D.; Bau, R.; Feng, J. *J. Am. Chem. Soc.* **1990**, *112*, 7619.
(20) Seppelt, K. *Inorg. Synth.* **1980**, *20*, 33.
(21) Christe, K. O.; Wilson, W. W. *J. Fluorine Chem.* **1990**, *47*, 117. Winfield, J. M. *J. Fluorine Chem.* **1984**, *25*, 91.

(22) Dunning, T. H., Jr.; Hay, P. J. In *Methods of Electronic Structure Theory*; Schaefer, H. F., III, Ed.; Plenum Press: New York, 1977; Chapter 1.
(23) Wadt, W. R.; Hay, P. J. *J. Chem. Phy.* **1985**, *82*, 284.
(24) Huzinaga, S.; Andzelm, J.; Klobukowski, M.; Radzio, E.; Sakai, Y. U.; Tatasaki, H. *Gaussian Bassi Sets of Molecular Calculations*; Elsevier: Amsterdam, 1984.
(25) (a) Komornicki, A.; Ishida, K.; Morokuma, K.; Ditchfield, R.; Conrad, M. *Chem. Phys. Lett.* **1977**, *45*, 595. (b) McIver, J. W., Jr.; Komornicki, A. *Chem. Phys. Lett.* **1971**, *10*, 202. (c) Pulay, P. In *Applications of Electronic Structure Theory*; Schaefer, H. F., III, Ed.; Plenum Press: New York, 1977; p 153.
(26) (a) Moller, C.; Plesset, M. S. *Phys. Rev.* **1934**, 46, 618. (b) Pople, J. A.; Binkley, J. S.; Seeger, R. *Int. J. Quantum Chem., Symp.* **1976**, *10*, 1.
(27) (a) King, H. F.; Komornicki, A. *J. Chem. Phys.* **1986**, *84*, 5465. (b) King, H. F.; Komornicki, A. In *Geometrical Derivatives of Energy Surfaces and Molecular Properties*; Jorgenson, P., Simons, J., Eds.; NATO AESI Series C; D. Reidel: Dordrecht, 1986; Vol. 166, p 207.
(28) Breidung, J.; Thiel, W.; Komornicki, A. *Chem. Phys. Lett.* **1988**, *153*, 76.
(29) GRADSCF is an ab initio program system designed and written by A. Komornicki at Polyatomics Research.
(30) Marsden, C. J. *J. Chem. Phys.* **1987**, *87*, 6626.
(31) (a) Parr, R. G.; Yang, W. *Density Functional Theory of Atoms and Molecules*; Oxford University Press: New York, 1989. (b) Salahub, D. R. In *Ab Initio Methods in Quantum Chemistry* II; Lawley, K. P., Ed.; J. Wiley & Sons: New York, 1987; p 447. (c) Wimmer, E.; Freeman, A. J.; Fu, C.-L.; Cao, P.-L.; Chou, S.-H.; Delley, B. In *Supercomputer Research in Chemistry and Chemical Engineering*; Jensen, K. F., Truhlar, D. G., Eds.; ACS Symposium Series No. 353; American Chemical Society: Washington, DC, 1987; p 49. (d) Jones, R. O.; Gunnarsson, O. *Rev. Mod. Phys.* **1989**, *61*, 689. (e) Zeigler, T. *Chem. Rev.* **1991**, *91*, 651.
(32) Andzelm, J.; Wimmer, E.; Salahub, D. R. In *The Challenge of d and f Electrons: Theory and Computation*; Salahub, D. R., Zerner, M. C., Eds.; ACS Symposium Series No. 394; American Chemical Society: Washington, DC, 1989; p 228. (b) Andzelm, J. In *Density Functional Methods in Chemistry*; Labanowski, J., and Andzelm, J., Eds.; Springer-Verlag: New York, 1991; p 101. Andzelm, J. W.; Wimmer, E. *J. Chem. Phys.* **1992**, *96*, 1280. DGauss is a local density functional program available via the Cray Research Unichem Project, Cray Research, Eagan, MN, 1993.
(33) Chen, H.; Krashowski, M.; Fitzgerald, G. *J. Chem. Phys.*, in press.
(34) Troullier, N.; Martins, J. L. *Phys. Rev. B* **1991**, *43*, 1993.
(35) Godbout, N.; Salahub, D. R.; Andzelm, J.; Wimmer, E. *Can. J. Chem.* **1992**, *70*, 560.

potential of Vosko, Wilk, and Nusair[36] and at the self-consistent nonlocal level with the exchange potential of Becke[37] together with the correlation functional of Perdew[38] (NLDFT/BP). Geometries were optimized by using analytical gradients.[32] Second derivatives were calculated by numerical differentiation of the analytic first derivatives. A two-point method with a finite difference of 0.01 au was used.

Results and Discussion

Synthesis. Although the results of our theoretical calculations (see below) suggest that XeF_7^+ is a stable species, its synthesis has so far not been achieved and is expected to be very difficult. The calculated oxidizer strength of XeF_7^+ is almost identical to that of KrF^+, which is the strongest presently known oxidative fluorinator.[39] Therefore, its synthesis from XeF_6 by oxidative fluorination will require an oxidizer that is stronger than KrF^+. The synthesis of XeF_7^+ from XeF_8 by F^- abstraction will be similarly difficult because XeF_8 is unknown and will also be very difficult to synthesize.

The synthesis of $N(CH_3)_4TeF_7$ is readily accomplished by the reaction of $N(CH_3)_4F$ with a moderate excess of TeF_6 in CH_3CN solution.

$$N(CH_3)_4F + TeF_6 \xrightarrow{CH_3CN} N(CH_3)_4TeF_7 \qquad (1)$$

The use of an excess of $N(CH_3)_4F$ must be avoided since it results in the formation of the TeF_8^{2-} anion.[18] The compound $N(CH_3)_4TeF_7$ is a stable, white, crystallinic material that can be recrystallized from CH_3CN. Two independent single-crystal X-ray diffraction studies,[9,40] have been carried out and yielded identical results. The TeF_7^- anion in $N(CH_3)_4TeF_7$ undergoes 4-fold disorder for the five equatorial fluorine ligands. Although these studies established for TeF_7^- a distorted, pentagonal bipyramidal structure in which the axial bonds are shorter than the equatorial bonds, the remaining structural features were not well determined because of the disorder.

NMR Spectra of TeF_7^-. The ^{125}Te NMR spectrum of $N(CH_3)_4TeF_7$ in CH_3CN at 30 °C shows[7,8] a binominal octet [$\delta(^{125}Te)$, 327.4 ppm; $^1J(^{125}Te-^{19}F)$, 2876 Hz]. This demonstrates the equivalence of all seven fluorine ligands on the NMR time scale due to a rapid intramolecular exchange mechanism which cannot be frozen out on cooling the sample down to –48 °C, the freezing point of the CH_3CN solution. The ^{125}Te chemical shift of TeF_7^- is significantly more shielded (i.e., by 217.8 ppm) than that of TeF_6 in CH_3CN at 30 °C [$\delta(^{125}Te)$, 545.2 ppm; $^1J(^{125}Te-^{19}F)$, 3746 Hz], and this is in accord with the expected trend of increasing shielding with increasing negative charge.[41]

The ^{19}F NMR spectrum of $N(CH_3)_4TeF_7$ in CH_3CN at 30 °C (Figure 1) is also consistent with the TeF_7^- anion undergoing a rapid intramolecular exchange process and displays a single environment [$\delta(^{19}F)$, 16.1 ppm] flanked by natural abundance (7.14%) ^{125}Te[$^1J(^{19}F-^{125}Te$, 2876 Hz] and (0.908%) ^{123}Te[$^1J(^{19}F-^{123}Te)$, 2385 Hz] satellites. The isoelectronic IF_7 molecule displays similar fluxional behavior and a single environment in the ^{19}F NMR spectrum.[42] At an external field strength of 11.744 T, the high-resolution ^{19}F NMR spectrum of the central line of the TeF_7^- resonance (Figure 2) displays the isotopic shift pattern arising from ^{19}F ligands bonded to the natural abundance spinless tellurium isotopes in the $^{130}TeF_7^-$ (33.80%), $^{128}TeF_7^-$ (31.69%),

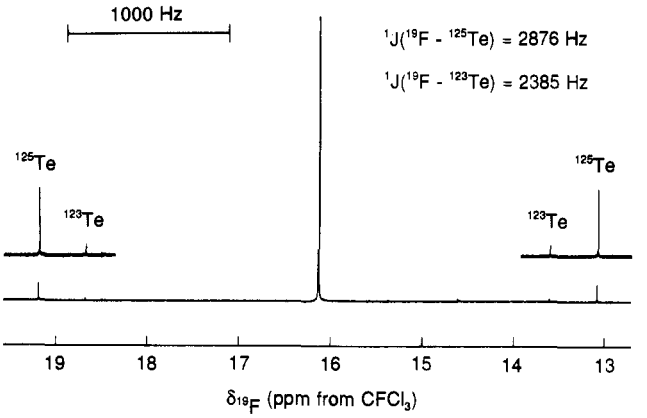

Figure 1. ^{19}F NMR spectrum (470.599 MHz) of $N(CH_3)_4TeF_7$ in CH_3CN solution at 30 °C.

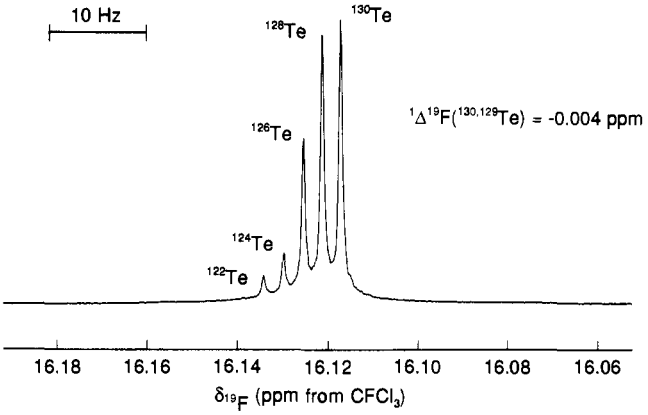

Figure 2. High-resolution ^{19}F NMR spectrum (470.599 MHz) of the central line of TeF_7^-.

$^{126}TeF_7^-$ (18.95%), $^{124}TeF_7^-$ (4.82%), and $^{122}TeF_7^-$ (2.60%) isotopomers. With every increase of two mass units, each isotopomer is shifted successively to low frequency by $^1\Delta^{19}F(Te)$ = –0.0042 ppm. This value is essentially identical, within experimental error, with values obtained for TeF_6 and various $OTeF_5$ derivatives.[43] The ^{19}F chemical shift of TeF_7^- is deshielded by 67.4 ppm with respect to that of TeF_6 in CH_3CN at 30 °C. The pentagonal planes of fluorine ligands in the XeF_5^- and IOF_6^- anions show similar high-frequency chemical shifts which have been suggested to arise from a low-energy HOMO excitation in the paramagnetic contribution to the ^{19}F shielding constant in these anions.[6,10] In TeF_7^-, the observed ^{19}F chemical shift represents a weighted average of the F_{ax} and F_{eq} chemical shifts (eq 2).

$$\delta(^{19}F)_{av} = {}^2/_7\delta(^{19}F_{ax}) + {}^5/_7\delta(^{19}F_{eq}) \qquad (2)$$

Nevertheless, the fact that this chemical shift occurs at significantly higher frequency than that of TeF_6 supports the idea that the five equatorial fluorines in TeF_7^- have a higher frequency ^{19}F shift than the two axial fluorines, since the former will contribute the larger weighting to the average chemical shift. In fact, it is possible to estimate, to a first approximation, the individual chemical shifts of the F_{ax} and F_{eq} environments of TeF_7^- in the absence of exchange. The chemical shift of the F_{ax} environment may be estimated from an observation made from the ^{19}F NMR spectrum of IOF_6^-, in which it is found that the chemical shift of the F-*trans*-to-O environment occurs very close to the F-*trans*-to-O environments in the octahedral IOF_5 and *cis*-$IO_2F_4^-$ species.[4] This is not surprising since the nature of the sp_z hybrid bonding in the F_{ax}—I═O moiety changes little as compared with that for the equatorial fluorines on going from IOF_5 to IOF_6^- (i.e., from

(36) Vosko, S. J.; Wilk, L.; Nusair, M. *Can. J. Phys.* **1980**, *58*, 1200.
(37) Becke, A. D. *Phys. Rev. A* **1988**, *38*, 3098. (b) Becke, A. D. In *The Challenge of d and f Electrons: Theory and Computation*; Salahub, D. R.; Zerner, M. C., Eds.; ACS Symposium Series No. 394; American Chemical Society: Washington, DC, 1989; p 166. (c) Becke, A. D. *Inter. J. Quantum Chem., Quantum. Chem. Symp.* **1989**, *23*, 599.
(38) Perdew, J. P. *Phys. Rev. B* **1986**, *33*, 8822.
(39) Christe, K. O.; Dixon, D. A. *J. Am. Chem. Soc.* **1992**, *114*, 2978.
(40) Mercier, H. C. P. Unpublished results.
(41) Jameson, C. J.; Mason, J. In *Multinuclear NMR*; Mason, J., Ed.; Plenum Press: New York, 1987; Chapter 3, pp 66–68.
(42) Gillespie, R. J.; Quail, J. W. *Can. J. Chem.* **1964**, *42*, 2671. Muetterties, E. L.; Packer, K. J. *J. Am. Chem. Soc.* **1964**, *86*, 293.
(43) Sanders, J. C. P.; Schrobilgen, G. J. To be submitted.

Table I. Observed and Calculated Vibrational Spectra of Isoelectronic TeF_7^-, IF_7, and XeF_7^+

assignment in point group D_{5h}		approximate mode description	TeF_7^- obsd freq, cm^{-1} (intens)		TeF_7^- calcd freq, cm^{-1} (IR intens)		IF_7 obsd freq, cm^{-1} (intens)		IF_7 calcd freq, cm^{-1} (IR intens)		XeF_7^+ calcd freq, cm^{-1} (IR intens)	
			Ra	IR	SCF[a]	NLDFT[b]	Ra	IR	SCF[a]	NLDFT[c]	SCF[a]	NLDFT[d]
A_1'	ν_1	ν sym XF_2 ax	640 (10)		644.6	648 (0)	676 (2)		673	670 (0)	681.6	684 (0)
	ν_2	ν sym XF_5 eq inphase	597 (2.6)		595.7	596 (0)	635 (10)		644	621 (0)	625.8	620 (0)
A_2''	ν_3	ν asym XF_2 ax		699 vs	703.0	713 (147)		746 s	753	752 (129)	757.1	776 (88)
	ν_4	δ umbrella XF_5 eq		335 ms	336.7	342 (51)		365 s	368	366 (37)	361.6	360 (23)
E_1'	ν_5	ν asym XF_5 eq		625 vs	618.4	614 (220)		670 vs	681	658 (232)	688.1	677 (158)
	ν_6	δ sciss XF_2 ax		385 s	387.7	377 (306)		425 vs	441	418 (204)	438.6	416 (137)
	ν_7	δ asym XF_5 eq in-plane		not obsd	236.5	238 (0.1)		257 w	265	267 (0.2)	270.1	267 (0)
E_1''	ν_8	δ wag XF_2 ax	295 (0.5) br		291.4	297 (0)	319 (0.6)		320	322 (0)	318.4	320 (0)
E_2'	ν_9	mixture of δ sciss XF_5 in-plane and ν asym XF_5 eq	not obsd		521.1	523 (1.0)	596 (0.2)		605	606 (0)	621.1	617 (0)
	ν_{10}		458 (1.6)		442.5	444 (11)	510 (1.7)		515	508 (0)	541.0	539 (0)
E_2''	ν_{11}	δ pucker XF_5			52.9	59 (0)	[68]		59	82 (0)	81.6	90 (0)

[a] Scaling factors used: TeF_7^-, stretching modes = 0.9293, deformation modes = 0.8810; IF_7, all modes = 0.9320; XeF_7^+, all modes = 0.93. [b] Scaling used: stretching modes, +38 cm^{-1}; deformation modes, −38 cm^{-1}; for the scaling, ν_9 was treated as the deformation mode and ν_{10} as the stretching mode in agreement with their PED. [c] Scaling used: stretching modes, +30 cm^{-1}; deformation modes, −10 cm^{-1}; ν_9 and ν_{10} are almost equal mixtures of stretching and bending and both were scaled as stretching modes. [d] Scaling used: stretching modes, +35 cm^{-1}; deformation modes, −15 cm^{-1}; ν_9 and ν_{10} were both scaled as stretching modes.

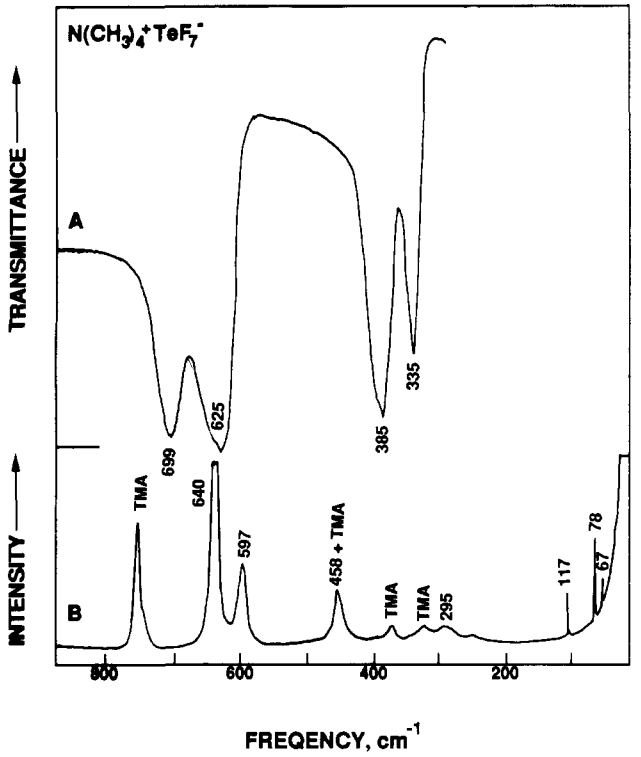

Figure 3. Infrared (trace A) and Raman (trace B) spectra of solid $N(CH_3)_4TeF_7$ recorded at room temperature. The Raman bands marked by TMA are due to the $N(CH_3)_4^+$ cation.

two three-center 4-electron bonds to a six-center 10-electron bond system), as has been demonstrated by recent ab initio calculations.[4] If the ideas behind the above ^{19}F shift observation are extrapolated to other pentagonal bipyramidal fluoro anions, then it can be anticipated that the F_{ax} environment of TeF_7^- will have an ^{19}F chemical shift close to that of TeF_6 (i.e., −51.3 ppm). Substitution of this value and the observed average ^{19}F chemical shift for TeF_7^- into eq 2 allows the chemical shift of F_{eq} to be estimated as 43 ppm. A similar calculation may be performed for IF_7 by using the observed average ^{19}F chemical shift for IF_7[$\delta(^{19}F)$, 172 ppm][44] and assuming that $\delta(F_{ax})$ will be close to the ^{19}F chemical shift of IF_6^+[$\delta(^{19}F)$, 73 ppm].[45] This yields the ^{19}F chemical shift for the F_{eq} environment of IF_7 as 212 ppm.

The magnitude of the one-bond ^{125}Te–^{19}F coupling constant drops from 3746 Hz in TeF_6 to 2876 Hz in TeF_7^-. The latter represents the average value of the $^1J(^{125}Te$–$^{19}F_{ax})$ and $^1J(^{125}Te$–$^{19}F_{eq})$ couplings, and its smaller magnitude probably reflects a correspondingly small value for $^1J(^{125}Te$–$^{19}F_{eq})$ arising from the weaker, more polar Te–F_{eq} bonds in the TeF_7^- anion.

Vibrational Spectra of TeF_7^-. The infrared and Raman spectra of solid $N(CH_3)_4TeF_7$ are shown in Figure 3. In addition to the bands due to TeF_7^-, that are denoted in Figure 3 by their frequency values, bands due to the $N(CH_3)_4^+$ cation have been observed, which are denoted by TMA. Since the vibrational spectra of $N(CH_3)_4^+$ are well-known and, for $N(CH_3)_4TeF_7$, are completely analogous to those previously reported and analyzed for the $N(CH_3)_4^+$ salts of F^-,[19] HF_2^-,[46] XeF_5^-,[6] IOF_6^-,[4] $TeOF_5^-$,[10] $TeOF_6^{2-}$,[10] or N_3^-,[47] only the bands due to TeF_7^- need to be analyzed. This goal was accomplished by a comparison of the observed spectra with those[3] of isoelectronic IF_7 and those calculated for the isoelectronic series XeF_7^+, IF_7, TeF_7^- by theoretical methods (see Table I).

Theoretical Calculations for XeF_7^+, IF_7, and TeF_7^-. The electronic structure calculations were done by both ab initio molecular orbital and density functional theories. The results are summarized in Tables I and II. There is only a small effect of correlation on the energy differences for IF_7 and TeF_7^-, but there is a larger effect for XeF_7^+. The size of the correlation correction to the energy difference seems to follow the congestion in the plane with the most congested structure XeF_7^+ having the largest correlation energy effect. It should be noted that the iodine pseudopotential for the self-consistent nonlocal density functional calculation was very difficult to generate due to the presence of "ghost" states.

Since the geometry and vibrational frequencies of IF_7 are well established,[3,48] the quality of our calculations can readily be examined. As can be seen from Table II, the use of a norm-

(44) Recorded for this work as a neat sample at 25 °C.
(45) Brownstein, M.; Selig, H. *Inorg. Chem.* **1972**, *11*, 656.
(46) Wilson, W. W.; Christe, K. O.; Feng, J.; Bau, R. *Can. J. Chem.* **1989**, *67*, 1898.
(47) Christe, K. O.; Wilson, W. W.; Bau, R.; Bunte, S. W. *J. Am. Chem. Soc.* **1992**, *114*, 3411.

Table II. Observed and Calculated D_{5h} Geometries of TeF_7^-, IF_7, and XeF_7^+

	TeF_7^-			IF_7			XeF_7^+	
		calcd			calcd		calcd	
	obsd	SCF	NLDFT[a]	obsd	SCF	NLDFT	SCF	NLDFT
$r(X-F_{ax})$, Å	1.790(17)	1.801	1.769	1.781	1.771	1.781	1.773	1.778
$r(X-F_{eq})$, Å	1.832(20)–1.903(39)	1.872	1.864	1.857	1.833	1.856	1.830	1.850

[a] The bond lengths calculated by the NLDFT method are usually slight longer than those obtained by the SCF method. The shorter values calculated by the NLDFT method for TeF_7^- are attributed to our difficulties of obtaining a good pseudopotential for tellurium.

Table III. Total Energies (au), Zero-Point Energies (kcal/mol) and Imaginary Frequencies (cm^{-1}) for the Pentagonal Bipyramidal (PB), Monocapped Trigonal Prismatic (MTP), and Monocapped Octahedral (MO) Structures of TeF_7^-, IF_7, and XeF_7^+

	MP-2	SCF			NLDFT/BP	
structure	total energy[a]	total energy	zero-pt energy[b]	imag freq	total energy	imag freq
TeF_7^- (PB)	−705.555 318	−704.187 658	10.46	none	−707.703 843	none
TeF_7^- (MTP)	−705.550 267	−704.181 746	10.47	89	−707.701 802	93
TeF_7^- (MO)	−705.549 676	−704.181 149	10.41	64e	−707.697 625	77e
IF_7 (PB)	−708.412 369	−707.033 247	11.34	none	−710.653 843	none
IF_7 (MTP)	−708.408 298	−707.027 062	11.38	93	−710.650 508	94
IF_7 (MO)	−708.407 948	−707.026 454	11.32	67e	−710.648 087	75e
XeF_7^+ (PB)	−711.696 478	−710.267 925	11.54	none	−714.049 856	none
XeF_7^+ (MTP)	−711.690 749	−710.258 962	11.49	108	−714.044 235	99
XeF_7^+ (MO)	−711.690 450	−710.258 116	11.42	78e	−714.042 066	79e

[a] Valence electrons only. [b] Scaled by 0.9.

Table IV. Relative Energies (kcal/mol) for the Pentagonal Bipyramidal (PB), Monocapped Trigonal Prismatic (MTP), and Monocapped Octahedral (MO) Structures of TeF_7^-, IF_7, and XeF_7^+.

structure	MP-2	SCF	NLDFT/BP
TeF_7^- (PB)	0	0	0
TeF_7^- (MTP)	3.2	3.7	1.3
TeF_7^- (MO)	3.5	4.1	3.9
IF_7 (PB)	0	0	0
IF_7 (MTP)	2.6	3.9	2.1
IF_7 (MO)	2.8	4.3	3.6
XeF_7^+ (PB)	0	0	0
XeF_7^+ (MTP)	3.6	5.6	3.5
XeF_7^+ (MO)	3.8	6.2	4.9

conserving pseudopotential for the central atom combined with the exchange potential of Becke[37] and the nonlocal correlation functional of Perdew[38] at the self-consistent nonlocal level (NLDFT/BP) exactly duplicates the experimental geometry of IF_7, while the ab initio SCF calculations using effective core potentials also result in a geometry which is close to the observed one. The scaled calculated frequencies obtained by both methods are also in excellent agreement with each other and the experimental values (see Table I) and demonstrate the quality of both types of calculations. The agreement between the scaled SCF and NLDFT/BP frequencies is also very good for TeF_7^- and XeF_7^+ (see Table I), and for TeF_7^-, the calculated frequencies duplicate well the observed ones.

As has been pointed out already in the Introduction, three structures which are very close in energy[15] exist for these heptacoordinated compounds. It was therefore of interest to calculate the total and relative energies of these structures (see Tables III and IV) and to determine their nature on the corresponding potential energy surfaces. Our results show that for all three members of the XeF_7^+, IF_7, TeF_7^- series the pentagonal bipyramid is the minimum energy structure, followed by the monocapped trigonal prism and the monocapped octahedron. Furthermore, they show that with increasing hardness, i.e., on going from the TeF_7^- anion to the smaller IF_7 molecule and XeF_7^+ cation, the energy gaps between the pentagonal bipyramid and the monocapped trigonal prism become larger and not smaller, as predicted by the energy law (1) of repelling points on a sphere.[13-15] This confirms our previously reached conclusion[3,4] that the pentagonal bipyramidal minimum energy structure of these heptacoordinated main group fluorides is not dictated by the hardness of the valence shell electron pair repulsion potential but by the geometry of the valence electron orbitals on the central atom.

Furthermore, our results show that the monocapped octahedron possesses a degenerate imaginary frequency and thus cannot be a transition state. The monocapped trigonal prism has only one imaginary frequency and, thus, is a transition state. Examination of the motion exhibited by the mode with the imaginary frequency shows that it is the motion expected for converting an axial F into an equatorial F. In fact, for XeF_7^+, if the convergence is tightened in the geometry optimization, the monocapped trigonal prism can relax to the pentagonal bipyramid. The small energy differences between the three lowest energy structures are in accord with the NMR experiments in which only one type of fluorine was observed, suggesting a low energy barrier toward axial–equatorial ligand exchange.

Normal Coordinate Analysis. The above given results from the theoretical calculations and their close agreement with the experimental vibrational spectra firmly establish their assignments. Inspection of Table I shows the expected frequency trends, i.e., a significant frequency increase with decreasing negative charge on the fluorine ligands which, on going from IF_7 to XeF_7^+, is partially counteracted by the fact that Xe–F bonds are generally weaker than the corresponding I–F bonds. The assignments for TeF_7^- given in Table I differ for ν_1, ν_2, ν_9, and ν_{10} from those tentatively made[7] in the absence of theoretical calculations.

A particularly interesting and originally most perplexing problem was making the assignments in the A_1' block. This block contains only two modes, the symmetric axial and the symmetric equatorial stretching modes, ν_1 and ν_2, respectively. Since their motions are orthogonal ($G_{12} = 0$) and the central atom is much heavier than the fluorine ligands, the two vibrations were expected to be highly characteristic and analogous for IF_7 and TeF_7^-. However, the observed Raman bands (i.e., IF_7, 676 cm^{-1} (Raman intensity of 2), 635 cm^{-1} (Raman intensity of 10); TeF_7^-, 640 cm^{-1} (Raman intensity of 10), 597 cm^{-1} (Raman intensity of 2.6)) show that either their relative frequencies or their intensities are reversed. Since generally the relative intensities are the more reliable guide for making assignments, we had assigned in our preliminary note[7] the more intense Raman bands, at 635 cm^{-1}

(48) Adams, W. J.; Bradford Thompson, H.; Bartell, L. S. *J. Chem. Phys.* **1970**, *53*, 4040.

Table V. Scaled SCF Force Fields[a] of the Isoelectric Series TeF_7^-, IF_7, XeF_7^+

assignment		TeF_7^- freq, cm^{-1}	TeF_7^- symmetry force constants	TeF_7^- PED	IF_7 freq, cm^{-1}	IF_7 symmetry force constants	IF_7 PED	XeF_7^+ freq, cm^{-1}	XeF_7^+ symmetry force constants	XeF_7^+ PED
A_1'	ν_1	644.6	$F_{11} = 4.460$ $F_{12} = 0.304$	$72S_1 + 28S_2$	673	$F_{11} = 5.063$ $F_{12} = -0.0058$	$100S_1$	681.6	$F_{11} = 5.134$ $F_{12} = -0.218$	$92S_1 + 8S_2$
	ν_2	595.7	$F_{22} = 4.160$	$72S_2 + 28S_1$	644	$F_{22} = 4.651$	$100S_2$	625.8	$F_{22} = 4.445$	$92S_2 + 8S_1$
A_2''	ν_3	703.0	$F_{33} = 4.361$ $F_{34} = 0.378$	$93S_3 + 7S_4$	753	$F_{33} = 4.947$ $F_{34} = 0.342$	$92S_3 + 8S_4$	757.1	$F_{33} = 4.958$ $F_{34} = 0.206$	$91S_3 + 9S_4$
	ν_4	336.7	$F_{44} = 1.413$	$100S_4$	368	$F_{44} = 1.624$	$100S_4$	361.6	$F_{44} = 1.582$	$100S_4$
E_1'	ν_5	618.4	$F_{55} = 3.429$ $F_{56} = -1.261$ $F_{57} = 0.278$	$98S_5 + 2S_7$	681	$F_{55} = 4.105$ $F_{56} = -1.427$ $F_{57} = 0.231$	$97S_5 + 3S_7$	688.1	$F_{55} = 4.162$ $F_{56} = -1.319$ $F_{57} = 0.126$	$95S_5 + 4S_6 + 1S_7$
	ν_6	387.7	$F_{66} = 3.137$ $F_{67} = -0.300$	$56S_6 + 35S_7 + 9S_5$	441	$F_{66} = 3.879$ $F_{67} = -0.318$	$62S_6 + 33S_7 + 5S_5$	438.6	$F_{66} = 3.799$ $F_{67} = -0.276$	$64S_6 + 33S_7 + 3S_5$
	ν_7	236.5	$F_{77} = 0.828$	$92S_7 + 8S_6$	265	$F_{77} = 0.980$	$93S_7 + 7S_6$	270.1	$F_{77} = 1.021$	$92S_7 + 7S_6 + 1S_5$
E_1''	ν_8	291.4	$F_{88} = 0.708$	$100S_8$	320	$F_{88} = 0.823$	$100S_8$	318.4	$F_{88} = 0.815$	$100S_8$
E_2'	ν_9	521.1	$F_{99} = 2.218$ $F_{9,10} = 0.468$	$77S_{10} + 23S_9$	605	$F_{99} = 3.436$ $F_{9,10} = 0.531$	$57S_{10} + 43S_9$	621.1	$F_{99} = 3.976$ $F_{9,10} = 0.462$	$68S_9 + 32S_{10}$
	ν_{10}	442.5	$F_{10,10} = 3.007$	$76S_9 + 24S_{10}$	515	$F_{10,10} = 3.375$	$61S_9 + 39S_{10}$	541.0	$F_{10,10} = 3.334$	$70S_{10} + 30S_9$
E_2''	ν_{11}	52.9	$F_{11,11} = 0.0548$	$100S_{11}$	59	$F_{11,11} = 0.0647$	$100S_{11}$	81.6	$F_{11,11} = 0.125$	$100S_{11}$

[a] The symmetry coordinates are identical to those used in ref 8 for IF_7; i.e. S_1 = sym ax stretch, S_2 = sym eq stretch, S_9 = asym eq stretch, S_{10} = δ asym XF_5 in-plane. Stretching force constants in mdyn/Å, deformation constants in mdyn Å/rad^2, and stretch–bend interaction constants in mdyn/rad. The following scaling factors were used for the force constants. TeF_7^-: stretching force constants = $(0.9293)^2 = 0.8636$; deformation constants = $(0.881)^2 = 0.776\ 16$; stretch–bend interaction constants = $(0.9293 \times 0.881) = 0.8187$. IF_7: all constants = $(0.932)^2 = 0.8686$. XeF_7^+: all constants = $(0.93)^2 = (0.8649)$.

Table VI. Detailed Normal Coordinate Analysis of the A_1' Blocks of TeF_7^-, IF_7, and XeF_7^+

	TeF_7^- ν_1	TeF_7^- ν_2	IF_7 ν_1	IF_7 ν_2	XeF_7^+ ν_1	XeF_7^+ ν_2
calcd freq, cm^{-1}	644	595.7	673	644	681.6	625.8
obsd rel Ra intens	10	2.6	2	10	---	---
interaction force constant F_{12} (mdyn/Å)	+0.304		-0.006		-0.218	
potential energy distribution (%)	72 axial str. + 28 equat. str.	72 equat. str. + 28 axial str.	100 axial str.	100 equat. str.	92 axial str. + 8 equat. str.	92 equat. str. + 8 axial str.
internal coordinate displacement vectors	0.849 S_1 + 0.528 S_2	0.849 S_2 - 0.528 S_1	1.0 S_1	1.0 S_2	0.960 S_1 - 0.278 S_2	0.960 S_2 + 0.278 S_1
approximate mode description	in-phase combination of S_1 and S_2	out-of-phase combination of S_2 and S_1	pure S_1	pure S_2	out-of-phase combination of S_1 and S_2	in-phase combination of S_2 and S_1
qualitative estimate of rel Ra intens	2(0.849) + 5(0.528) = 4.329	5(0.849) - 2(0.528) = 3.189	2(1) = 2	5(1) = 5	2(0.96) - 5(0.278) = 0.53	5(0.96) + 2(0.278) = 5.356

in IF_7 and 640 cm^{-1} in TeF_7^-, to the symmetric equatorial stretch and the less intense ones, at 676 cm^{-1} in IF_7 and 597 cm^{-1} in TeF_7^-, to the symmetric axial stretch. The results of our ab initio force field calculations and normal coordinate analysis (see Table V), however, clearly show that in IF_7 and TeF_7^- the 676 and 640 cm^{-1} Raman bands, respectively, are the symmetric axial stretches and the 635 and 597 cm^{-1} bands, respectively, are the symmetric equatorial stretches. Consequently, it is the relative Raman intensities of ν_1 and ν_2 and not their frequencies that are reversed.

This intensity reversal can be rationalized by a more detailed inspection of the normal coordinate analysis data for the A_1' blocks of XeF_7^+, IF_7, and TeF_7^- (see Table VI). In IF_7, the F_{12} interaction force constant is essentially zero, ν_1 and ν_2 are pure axial and equatorial stretching, respectively, and the equatorial stretching mode, which involves five fluorine ligands, has a higher Raman intensity than the axial one, which involves only two fluorines. In TeF_7^-, the F_{12} interaction force constant has a substantial, positive value which results in ν_1 and ν_2 becoming 72/28% and 28/72% mixtures of axial and equatorial stretching, respectively. The signs of the internal displacement vectors show that, in TeF_7^-, ν_1 is an in-phase combination of the symmetry coordinates S_1 and S_2 and ν_2 their out-of-phase combination. The lower frequency and energy of the out-of-phase combination is in accord with our expectations from mutual ligand repulsion arguments that a shortening of the equatorial bonds should result in increased repulsion and, therefore, in a lengthening of the axial bond. This same feature has previously been found and discussed for the A_1' block of the closely related, trigonal bipyramidal PF_5 molecule of D_{3h} symmetry.[30]

For XeF_7^+, the situation is reversed, i.e., F_{12} becomes negative and, as a result, axial stretching encourages equatorial stretching. The exact nature of this effect, which is opposite to the mutual repulsion effect, is not entirely clear at this time but is believed to be electronic in nature. It seems to increase with an increasing positive charge on the species, i.e., in the direction $TeF_7^- \rightarrow IF_7 \rightarrow XeF_7^+$.

The internal relationships between the diagonal and interaction force constants, the potential energy distribution, and in-phase and out-of-phase combinations of the symmetry coordinates for the A_1' blocks of these D_{nh} bipyramidal molecules can be more

fully understood by an inspection of the plots of the diagonal force constants F_{11} and F_{22} as functions of their interaction

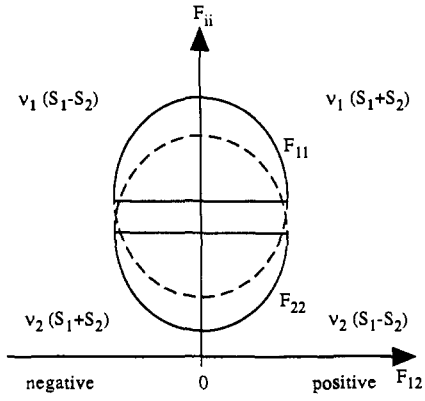

constant F_{12}. The possible solutions of F_{11} and F_{22} have the form of ellipses whose centers for the off-diagonal kinetic energy term G_{12} being zero, as is the case for these D_{nh} molecules,[49] are located on the F_{ii} axis.[50]

From this graph, it is obvious that, for $G_{12} = 0$, F_{12} does not also automatically become zero, as has sometimes been incorrectly assumed in previous force field calculations. If $F_{12} = 0$, then F_{11} and F_{22} are a maximum and a minimum, respectively, and ν_1 and ν_2 are 100% characteristic vibrations, i.e., no mixing of the symmetry coordinates occurs, as is the case for IF_7. If F_{12} is nonzero, the numerical values of F_{11} and F_{22} depend only on the size of F_{12} but not on its sign. The sign of F_{12}, however, determines whether ν_1 or ν_2 is the inphase combination of the symmetry coordinates S_1 and S_2 and, therefore, determines their relative Raman intensities. A negtive F_{12} value results in the higher frequency vibration being the out-of-phase combination of S_1 and S_2 and having a decreased Raman intensity. This logic is confirmed by the rough estimates of the relative Raman intensities of ν_1 and ν_2, made in Table VI under the assumption that the polarizabilities of the equatorial and the axial fluorine ligands are identical. These rough estimates are in reasonable agreement with the relative Raman intensities observed for TeF_7^- and IF_7 and confirm the observed intensity reversal. Unfortunately, the ultimate question, what makes F_{12} change its sign on going from TeF_7^- to XeF_7^+, cannot be answered with confidence at this time.

One final observation for the XeF_7^-, IF_7, TeF_7^+ series concerns the identities of the antisymmetric equatorial stretching mode ν_9 and the equatorial in-plane deformation ν_{10}. As can be seen from the potential energy distributions of Table V, these two vibrations have similar frequencies and are strongly mixed. In TeF_7^-, the stretching vibration has the lower frequency, whereas in XeF_7^+, it has the higher frequency. The fact that in TeF_7^- the frequency and antisymmetric stretching force constants drop below those of the antisymmetric, in-plane deformation can be explained by the lengthening and weakening of its equatorial Te–F bonds due to the formal negative charge which increases the ionicity of these bonds.

Conclusion

The results of this study show that for all three members of the isoelectronic XeF_7^+, IF_7, TeF_7^- series the pentagonal bipyramid is the minimum energy structure and the monocapped trigonal prism is a transition state. This finding supports our previous proposal[3,4,10] that the pronounced preference of heptacoordinated main-group element compounds for pentagonal bipyramidal structures is not caused by their relative hardness but is best explained by the geometry of the valence electron orbitals of their central atoms. This geometry is the result of a bonding scheme involving a planar, delocalized p_{xy} hybrid of the central atom for the formation of five equatorial, semi-ionic, six-center 10-electron bonds and an sp_z hybrid for the formation of two mainly covalent axial bonds.[3] In addition, the Raman intensities in the A_1' block of TeF_7^- and IF_7 exhibit an unprecedented intensity reversal, which suggests the existence of an electronic effect which counteracts the intuitively obvious ligand–ligand repulsion effect of axial bond shortening encouraging equatorial bond lengthening.

Acknowledgment. The authors thank Dr. E. C. Curtis, Dr. C. J. Schack, and Mr. R. D. Wilson for their help and fruitful discussions. The work at Rocketdyne was financially supported by the U.S. Air Force Phillips Laboratory and the U.S. Army Research Office, and that at McMaster University, by the U.S. Air Force Phillips Laboratory and the Natural Sciences and Engineering Research Council of Canada.

(49) Ohwada, K. *Spectrochim. Acta, Part A* **1981**, 37A, 873.
(50) Sawodny, W. *J. Mol. Spectrosc.* **1969**, *30*, 56.